International Journal of Biological Macromolecules 282 (2024) 136159

Contents lists available at ScienceDirect

International Journal of Biological Macromolecules

journal homepage: www.elsevier.com/locate/ijbiomac

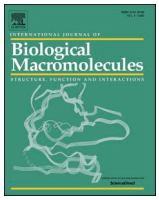

Research Paper

Side-chain-induced changes in aminated chitosan: Insights from molecular dynamics simulations

Henrik Schopmans [a,b], Tillmann Utesch [c], Patrick Théato [d,e], Maria Andrea Mroginski [f], Mariana Kozlowska [a,*]

[a] Institute of Nanotechnology, Karlsruhe Institute of Technology, Kaiserstr. 12, 76131 Karlsruhe, Germany
[b] Institute of Theoretical Informatics, Karlsruhe Institute of Technology, Kaiserstr. 12, 76131 Karlsruhe, Germany
[c] Leibniz-Forschungsinstitut für Molekulare Pharmakologie im Forschungsverbund Berlin e.V. Campus, Berlin-Buch Robert-Roessle-Str. 10, 13125 Berlin, Germany
[d] Institute for Chemical Technology and Polymer Chemistry, Karlsruhe Institute of Technology, Kaiserstr. 12, 76131 Karlsruhe, Germany
[e] Soft Matter Synthesis Laboratory, Institute for Biological Interfaces III, Karlsruhe Institute of Technology, Kaiserstr. 12, 76131 Karlsruhe, Germany
[f] Institute of Chemistry, Technical University Berlin, Str. des 17. Juni 135, 10623 Berlin, Germany

ARTICLE INFO

Keywords:
Chitosan
Amination
Water binding
Hydrogen bonding
Molecular dynamics simulation

ABSTRACT

Chitosan is a functional polymer with diverse applications in biomedicine, agriculture, water treatment, and beyond. Via derivatization of pristine chitosan, its functionality can be tailored to desired applications, e.g. immobilization of biomolecules. Here, we performed molecular dynamics simulations of three aminated chitosan polymers, where one, two, and three long-distanced side chains have been incorporated. These polymers have been previously synthesized and their properties were investigated experimentally, however, the observed dependencies could not be fully explained on the molecular level. Here, we develop a computational protocol for the simulation of functionalized chitosan polymers and perform advanced analysis of their conformational states, intramolecular interactions, and water binding. We demonstrate that intra- and intermolecular forces, especially hydrogen bonds induced by polymer side chain modifications, modulate dihedral angle conformational states of the polymer backbone and interactions with water. We explain the role of the chemical composition of the functionalized chitosans in their tendency to collapse and reveal the key role of the protonation of the amino group near the polymer backbone on the reduction of polymer collapse. We demonstrate that specific binding of water molecules, especially the intermediate water, is more pronounced in the polymer exhibiting such an amino group.

1. Introduction

Chitin is the second most abundant biopolymer (next to cellulose) [1] that is widely distributed in nature, especially in the shells of crustaceans. Chitosan (CS), i.e., poly-(D)-glucosamine, is a primary derivative of chitin that is obtained by deacetylation of chitin. Since chitin is one of the most produced organic materials annually by biosynthesis [2], CS poses a remarkable renewable resource with an impressive number of studies reported.

Chitin is a polysaccharide built from β-(1–4) linked 2-acetamide-2-deoxy-β D-glucopyranose (GlcNAc) units, while CS is obtained by (partial) alkaline deacetylation of chitin, replacing the acetamide group with an amino group (Fig. 1) [2,3]. Due to its specific structure and polycationic form at pH below 6.5–6.8, CS exhibits superb chemical and biological properties, which are used in a wide range of applications such as chelating agents [4–6], adsorbents [7,8], or matrices in nanobiocomposites [9,10]. It is known to possess specific properties such as solubility in various media, mucoadhesivity, polyoxysalt formation, polyelectrolyte behavior, the ability to form films, and optical and structural characteristics, as summarized in numerous available reviews, e.g. Ref. [11–13]. Due to its non-toxicity, exceptional biocompatibility, biodegradability, and strong affinity towards immobilization of biomolecules [14,15], it has been successfully used in the fabrication of biosensors [11,16–18] and beyond. Furthermore, chitosan's functional groups - two hydroxy groups and one amino group - can be chemically modified, allowing for improved properties towards desired applications, while maintaining its biochemical properties. Therefore, diverse CS modification strategies were reported [19–23]. The specific structure

* Corresponding author.
E-mail address: mariana.kozlowska@kit.edu (M. Kozlowska).

https://doi.org/10.1016/j.ijbiomac.2024.136159
Received 31 May 2024; Received in revised form 23 September 2024; Accepted 29 September 2024
Available online 30 September 2024

of CS enables chemical and physical modifications by preparation of nanoparticles, microspheres, hydrogels (beads, membranes, films), or nanosheets [24].

While chitosan is used and studied experimentally in numerous ways, a microscopic view of its interactions and properties can be elaborated with the use of molecular simulations. Quantum mechanical calculations can be used to reveal interactions between CS repeat units and functional molecules [25–27]. However, due to the limitation of the system size, molecular mechanics has been a workhorse for chitosan simulations. Diverse pristine CS systems [28–32] as well as modified CS [33,34] have been simulated up to now. In most cases, adsorption processes [35–39], aggregation [40,41], binding of macromolecules [42,43], encapsulation [44], and wrapping [45] processes have been studied. Dissipative particle dynamics was applied to CS emulsion stabilisation [46]. Even if pristine CS is well studied from a computational point of view, understanding the molecular bases of its derivatives' functionality is still scarce. This is likely connected to the force field parameterization, i.e. the parameters of chemical modifications of chitosan are not available in standard force field potentials and their careful validation is necessary.

One of the examples of not fully understood microscopic properties of functionalized chitosan, observed in experimental studies, was reported for aminated CS [15,47]. There, three chitosan derivatives with different amounts (one to three) of long-distanced amino and imine groups in each repeat unit were introduced. The authors demonstrated the functionality of the modified polymers (attached to magnetic nanoparticles) to bind human serum albumin (HSA) [15]. By performing various analyses, they observed that the properties of the modified CS with two side chain modifications (called CS-Et(NH_2)$_2$) differ from the polymers with one or three long-distanced side chains. It is more hydrophilic, binds more water, and is thermally more stable. Moreover, it shows the lowest binding of HSA on the CS-coated nanoparticles. They observed different aggregation patterns of this polymer from molecular dynamics (MD) simulations and they assumed it was a reason for the smaller total surface area of CS-Et(NH_2)$_2$, which was confirmed experimentally. Therefore, the CS amino groups on the surface could not be actively involved in the binding of HSA. Yet, details of the conformational changes of the aminated polymers, as well as an in-depth explanation of water binding phenomena were not reported.

In this paper, we provide a detailed analysis of the time evolution of CS structural changes and chain morphology as a result of the chemical modification by the long-distanced side chains via three types of amination processes. Using all-atom MD simulations with adapted parameterization, we correlate the dynamics of CS in water with intramolecular and intermolecular interactions. Through a set of diverse analyses, with a special focus on formed hydrogen bonds, we deliver the reasoning for the unexpected behavior of CS derivatives in the reported experiments [15,47]. Moreover, chitosan interactions with water in neutral and protonated states are explained, providing a missing piece of information in the understanding of the hydrophilic properties of the studied CS derivatives.

2. Computational details

Three types of modified CS polymers, as reported previously [47] (see Fig. 1(b)), were simulated considering 20 repeat units and 80 % degree of deacetylation (DD). Fig. 1(c)-(e) shows parts of the chains of the three different modifications. Simulated models of the macromolecules included both neutral and protonated CS. No intermediate systems were simulated since the protonation states of the aminated side chains of CS were not reported experimentally. The pK_a value of chitosan is around 6.3–7.0 [2,4,11], while for the primary amino groups it is around 9–11, depending on the surrounding environment. Furthermore, the modified CS were synthesized in the alkalic conditions [47], which may

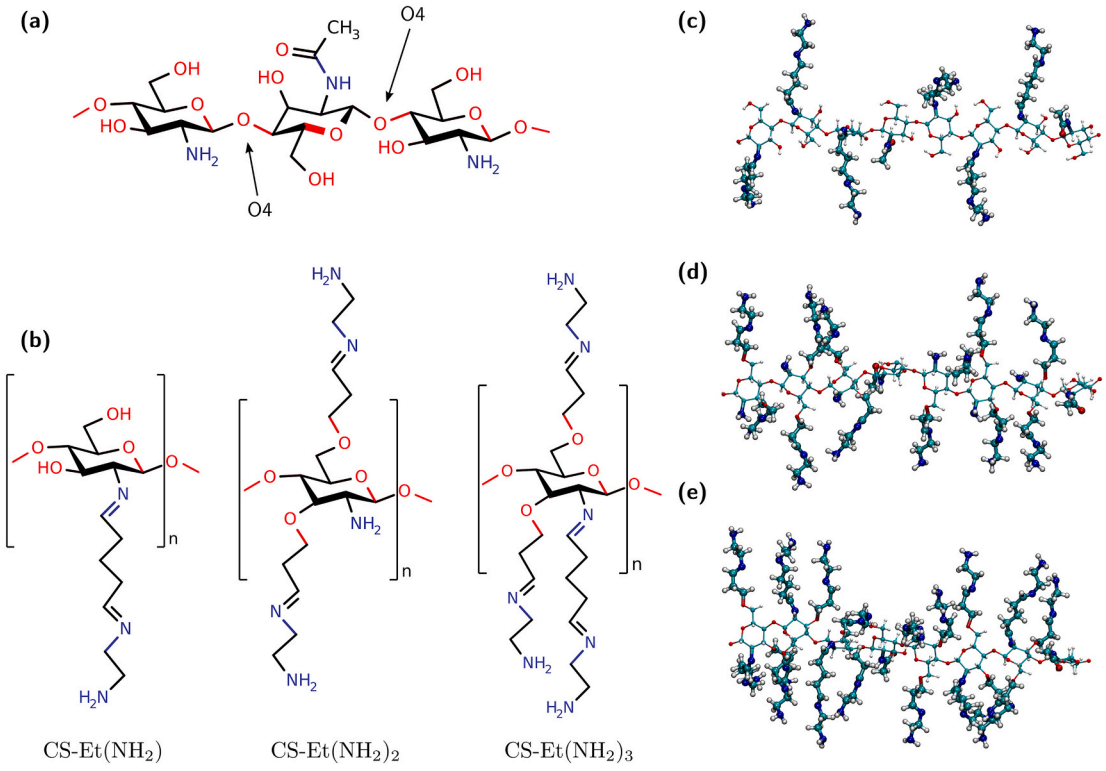

Fig. 1. (a) A schematic representation of a chitosan polymer. Repeat units for chitosan (GlcN) and chitin (GlcNAc) are demonstrated since the deacetylation process is, usually, not perfect [2] (degree of deacetylation DD ≠ 100 %). Oxygen atoms labeled as O4, which appear in Fig. 2, are marked for clarity. (b) The three aminated derivatives of chitosan investigated in this work (in the neutral form), CS-Et(NH_2), CS-Et(NH_2)$_2$, and CS-Et(NH_2)$_3$. (c)-(e) 3D models of the three systems, CS-Et(NH_2), CS-Et(NH_2)$_2$, and CS-Et(NH_2)$_3$, respectively. A fraction of the simulated polymers is depicted.

impact the polymer chain in packing and protonation capabilities, therefore, different protonation in CS models was considered. Neutral CS are labeled as CS-Et(NH_2), CS-Et(NH_2)$_2$, and CS-Et(NH_2)$_3$, while the protonated forms are labeled as CS-Et(NH_3^+), CS-Et(NH_3^+)$_2$, and CS-Et(NH_3^+)$_3$, respectively. Only in the case of CS with two side chain modifications we considered the semi-protonated state (CS-Et(NH_2)(NH_3^+)) in addition. Here, the two long-distanced amino groups were protonated, while the amino group near the backbone was not protonated. We considered such an intermediate system because the polymer with two modified side groups demonstrated significantly different properties among all cases studied [15,47]. To mimic the deacetylation level found in the experiment (75 % to 80 %), the polymers include 20 % evenly spaced chitin (GlcNAc) units without any modifications. It should be noted that even if low-molecular-weight CS was utilized in experiments, the simulated CS models represent shorter polymer fragments, aiming to understand the molecular bases of the dependencies observed. In addition, 100 % degree of derivatization was applied, however, the exact value is hard to derive for different CS chains in a material.

2.1. Polymer model

In this study, we used the CHARMM Additive All-Atom Force Field (FF) for Carbohydrate Derivatives (CHARMM36) [48,49] to describe potential functions of pristine chitin and chitosan. The parameters of the modified, long-distanced aminated side chains were generated using the CHARMM General Force Field (CGenFF version 1.0.0 using force field version 3.0.1) through ParamChem web-server [50–52]. For that, repeating subunits of the modified sugars CS-Et(NH_2) and CS-Et(NH_2)$_3$ (as depicted in Fig. 1(b)) and their protonated forms were used. The force field parameters, which were missing in the CHARMM FF for carbohydrates, were added to the main FF. The topology of long-distanced side chain chitosan modifications was added as patches to the BGLCNA residue (the name of the chitin units in the CHARMM FF), linked by equatorial-equatorial 1 → 4 glycosidic bonds (patch 14bb), using the CHARMM program (version 39b2). The generated polymer parameter files, as well as customized force field files, are available at the DOI: 10.17172/NOMAD/2024.05.31-1. Finally, coordinate and structure files of the modified chitosan polymers generated, necessary for further MD simulations using the Nanoscale Molecular Dynamics (NAMD) [53] software, were obtained with the visual molecular dynamics [54] (VMD, version 1.9.3) psfgen plugin utilizing CHARMM input files.

2.2. Molecular dynamics simulations

MD simulations were performed in the NPT ensemble using the NAMD program package (version 2.13 with GPU/CUDA). Polymers (one chain per simulation) were solvated with explicit water using the solvate plugin of the VMD software package. The TIP3P water model was used for all simulations. A cuboid simulation box with a minimum distance of 30 Å between the polymer and each face of the box was generated, resulting in a 30 Å thick layer of water surrounding the polymer in every direction. Neutralization of the systems with Cl^- ions was performed using the VMD Autoionize Plugin. The type and quantity of molecules simulated and the simulation box dimensions after the equilibration of each of the CS systems are listed in Table S1.

All simulations were performed using the periodic boundary conditions (PBC) in combination with the Particle Mesh Ewald (PME) method for electrostatic interactions. A cutoff of 12 Å, which determines the distance at which short-range forces become long-range forces in Ewald summation (grid spacing 1 Å) was applied. Non-bonded forces were calculated in every step, while pair-list distances till 16 Å were updated every 10 steps. Hydrogen atom vibrations were constrained using the ShakeH algorithm, therefore, the MD timestep of 2.0 fs was used. Langevin dynamics was used at $T = 300$ K with the pressure control by a Nosé-Hoover Langevin piston. It was set to normal pressure with a period of 200 fs and a damping time constant of 50 fs. The velocity Verlet algorithm was used to integrate all equations of motion.

Each MD simulation was started with initial energy minimization over 34,000 steps. During minimization, the polymer was first harmonically restrained to its initial state, so that water could adjust to the polymer. Then, we gradually removed the restraints. After minimization, the velocities were initialized at 100 K, after which the system was gradually heated to 300 K in steps of 25 K. Again, the polymer was restrained during heating and the restraints were removed after heating. An equilibration phase of 600 ps followed. The subsequent MD production run for each of the systems was 200 ns long. The coordinates and energies of the whole system were recorded every 2500 simulation steps (every 5 ps).

3. Results and discussion

3.1. Conformational states of chitosan

To evaluate the parameterization performed for the aminated chitosan derivatives and to estimate the impact of the side chain modifications on the chitosan torsion dynamics, two main dihedral angles of CS were examined. Typically, the φ angle denotes the H1′-C1′-O4-C4 dihedral angle connecting two monosaccharide units, while the ψ angle is the C1′-O4-C4-H4 dihedral angle, as visualized in Fig. 2(a). Fig. 2(d) represents the free energy, ΔG, as a function of these dihedral angles in the case of CS-Et(NH_2). (Free energy plots of the other modified CS polymers are depicted in Figs. S1 and S2.) ΔG was calculated from the probability density $P(\varphi,\psi)$ on a 150 × 150 grid as $\Delta G = -k_B T \ln(P(\varphi,\psi))$ using the MD trajectory of 200 ns. Based on this probability distribution, three types of backbone conformation of CS can be described, the *syn*, *anti-ψ*, and *anti-φ* states [29]. The *syn* conformation of pristine CS is defined by $-90° \leq \varphi \leq 125°$ and $-100° \leq \psi \leq 90°$. *anti-ψ* is defined by $\psi > 90°$ or $\psi \leq -100°$ and *anti-φ* by $\varphi > 125°$ or $\varphi \leq -100°$. We can see that the conformational states of the backbone are correctly represented in comparison to the dynamics of pristine chitosan reported by Tsai et al. [29]. In addition, the degree of the dihedral angle change in the aminated CS is smaller than in the pristine chitosan. As an example, ψ angles in the range of −180° to 180° can be found in pristine CS, while values in the range from approximately 60° to 125° are not sampled in the modified CS systems. This indicates additional structural constraints in the polymer dynamics, which are based on the significantly larger size of the aminated side chains that modulate the structural movements of polymers in water.

Analogously to the findings in pristine CS [29], the population of the two main distinct minima, *syn* and *anti-ψ* states, occurs (Fig. 2(d)). At $\varphi \approx 150°$, we also find the third CS conformer, the *anti-φ* state. However, the population of this minimum is rather small in all systems (also for pristine CS [29]), and is, therefore, not considered for further discussion. The comparisons demonstrate that the parameterization of the long-distanced side chains of CS and parameter integration in the carbohydrate FF correctly mimic the dynamical change of glycosidic bonds of the pristine CS backbone.

3.2. Dynamics of modified CS in solution

The exemplary structural changes of the modified CS derivatives (in neutral form) simulated at 300 K over a part of the full 200 ns MD are depicted in Fig. 3. The changes over the whole simulation time, including the results of the protonated polymers, are depicted in Figs. S3 and S4. We used the radius of gyration as a measure of the overall size of the polymer and its dynamics.

In Fig. 3, we observe that the radius of gyration ranges from 16 Å, indicating a collapsed chain, to values around 30 Å, corresponding to a fiber-like structure of the polymer. CS-Et(NH_2) attains linear chain conformations more frequently than the other considered macromolecules. Since there is only one side chain modification added, its

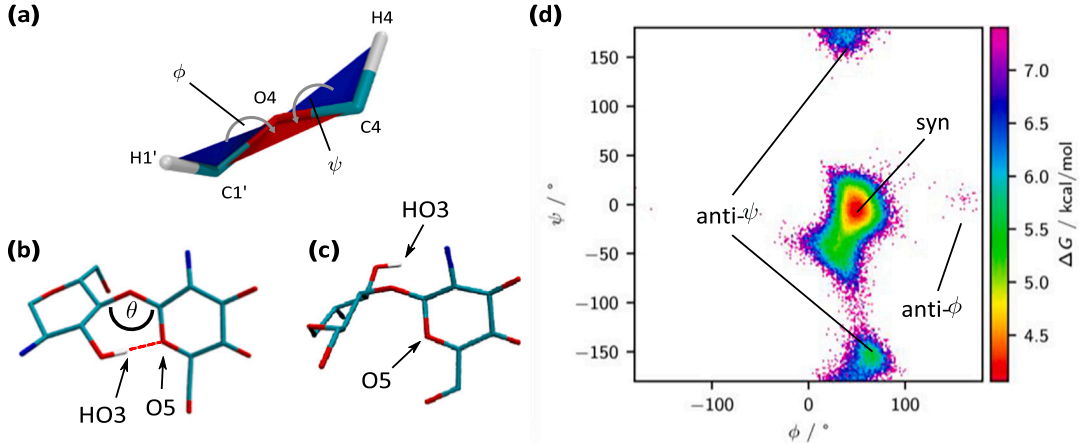

Fig. 2. (a) The definition of dihedral angles φ and ψ of CS. (b) Fragment of the disaccharide backbone of CS-Et(NH_2) in the *syn* state. The hydrogen bond between HO3 and O5, stabilizing the *syn* state, is marked with the red, dashed line. (c) Fragment of the disaccharide backbone of CS-Et(NH_2) in the *anti-ψ* state. (d) Free energy, ΔG, of CS-Et(NH_2) as a function of φ and ψ. The states *syn*, *anti-ψ*, and *anti-φ* are marked.

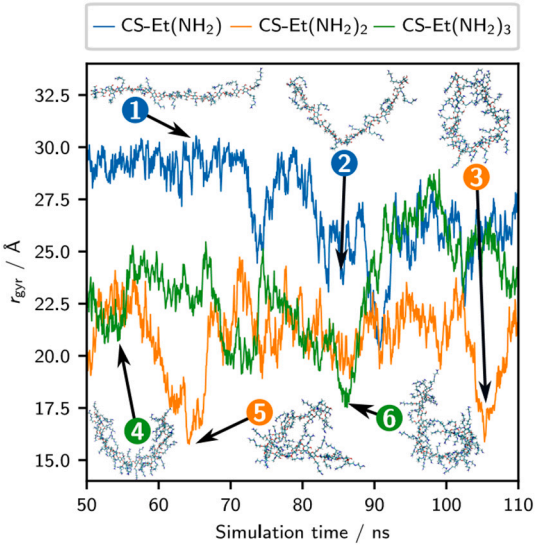

Fig. 3. The change of the radius of gyration r_{gyr} over time for polymers in the neutral state. To show the most relevant structural changes, a 60 ns fragment of the full 200 ns (see Fig. S3) is shown. Several snapshots of polymer structures formed are depicted.

dynamics resemble pristine CS [29]. However, more structural flexibility in comparison to the ideally linear form of CS-Et(NH_2) is also noticeable (see Fig. S3).

Different behavior is seen for CS-Et(NH_2)$_2$ and CS-Et(NH_2)$_3$: the tendency of polymer collapse is demonstrated by a significantly lower radius of gyration r_{gyr}. Structures "3", "5", and "6" in Fig. 3 denote the form of polymers upon the change of the radius of gyration. Surprisingly, CS-Et(NH_2)$_2$ is the only system where dense circle-like coils are observed (see structure "3"), showing evidence for small pore formation. This was not observed for CS-Et(NH_2). CS with three long-distanced side chains is probably too densely functionalized and the simulated chains are too short to observe similar events. The behavior of CS-Et(NH_2)$_2$ in comparison to CS-Et(NH_2) can be explained by different locations of the modified side chains (see Fig. 1), i.e. side chains in CS-Et(NH_2)$_2$ are denser and interactions between the neighboring chains, belonging to different repeat units, may occur. This would explain the higher degree of collapse of this polymer. Such interactions will be analyzed in more detail in the next sections.

Changes in the radius of gyration of the protonated CS polymers are depicted in Fig. S4. It is clearly seen that the polymers tend to be more linear-like due to the repulsive character of electrostatic interactions induced by protonation. The semi-protonated form CS-Et(NH_2)(NH_3^+), lacking the protonation on the amino group close to the CS backbone, shows the most significant collapsing events among the systems considered.

To demonstrate the general trend of structural changes between different modified CS, the probability density of the radius of gyration was calculated. Fig. 4(a) shows the probability density for the neutral polymers, Fig. 4(b) for the protonated systems. Lower values of the radius of gyration are noticeable for the neutral forms because the repulsive interactions are missing. Dominant collapsing of CS-Et(NH_2)$_2$ with the lowest values of r_{gyr} (an average r_{gyr} of 21.52 ± 0.01 Å, see Table 1) and a more fiber-like structure of CS-Et(NH_2) can be revealed. Smaller surface area of CS-Et(NH_2)$_2$, in comparison to the other two CS polymers, was also postulated in Ref. [15].

A more linear form of the protonated CS polymers is clearly seen in Fig. 4(b): generally, higher values of the radius of gyration (than calculated for the neutral systems) occur. However, the polymers with two long distanced modifications, CS-Et(NH_3^+)$_2$ and CS-Et(NH_2)(NH_3^+), feature a smaller average radius of gyration than the CS-Et(NH_3^+) and CS-Et(NH_3^+)$_3$ systems (27.19 ± 0.01 Å and 26.70 ± 0.01 Å, see Table 1, and orange and red curves in Fig. 4(b)). Moreover, two separated peaks are noticeable. This may indicate that even with the polymer protonation, some tendency to collapse still occurs and is probably modulated by the interplay of diverse intra- and intermolecular interactions, as well as the counter-ions. We have to note that the performed simulations do not include the impact of ionic strength. Modulating additional salt conditions in the system may change the behavior of the protonated CS, probably resembling the dynamics of the neutral systems, as was reported for pristine CS [29].

The persistence length l_p of modified CS, which indicates the length of the polymer over which its structure remains correlated (see Eq. 1 in SI), was also calculated. Together with the end-to-end distance (distance between terminal hydrogen atoms), r_{NN}, of the polymers (listed in Table 1), it shows that the neutral CS-Et(NH_2)$_2$ is the most flexible macromolecule, with l_p of 19.35 Å and an average r_{NN} of 57.11 ± 0.07 Å. The persistence length of CS-Et(NH_2) is the highest (45.87 Å), indicating less structural diversity of the polymer in comparison to the species with a higher number of long-distanced aminated side chains.

A significant change in the value of the persistence length and the end-to-end distance of the polymers is notable upon protonation. For the persistence lengths of the protonated systems, we find l_p = 112.74 Å for

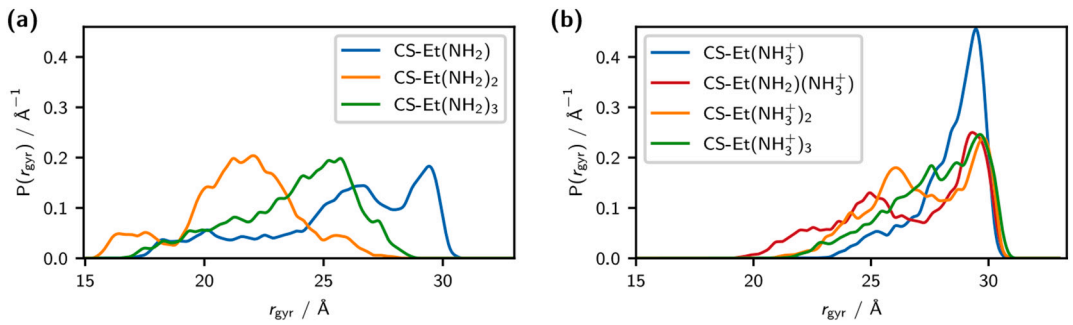

Fig. 4. Probability density of the radius of gyration r_{gyr} for neutral systems (a) and for protonated systems (b) calculated over 200 ns.

Table 1
Summary of the structural parameters of aminated CS from MD simulations of 200 ns: Persistence length l_p, average end-to-end distance (distance between terminal hydrogen atoms) $\langle r_{NN}\rangle$, average radius of gyration $\langle r_{gyr}\rangle$, population of the two main dihedral angle states, *syn* and *anti-ψ*, and the total number of HO3-O5 hydrogen bonds. For $\langle r_{NN}\rangle$ and $\langle r_{gyr}\rangle$ we further specify the standard error.

System	l_p/Å	$\langle r_{NN}\rangle$/Å	$\langle r_{gyr}\rangle$/Å	*syn*/ %	*anti-ψ*/%	HO3-O5 H-bonds
CS-Et (NH_2)	45.87	76.06 ± 0.10	25.69 ± 0.02	92.29	7.71	230,069
CS-Et (NH_3^+)	112.74	90.92 ± 0.04	28.36 ± 0.01	94.83	5.18	227,675
CS-Et (NH_2)$_2$	19.35	57.11 ± 0.07	21.52 ± 0.01	75.12	24.87	73,804
CS-Et (NH_2) (NH_3^+)	71.18	82.69 ± 0.07	26.70 ± 0.01	90.84	9.15	62,009
CS-Et (NH_3^+)$_2$	76.80	83.79 ± 0.06	27.19 ± 0.01	85.97	14.04	35,540
CS-Et (NH_2)$_3$	26.36	64.21 ± 0.08	23.74 ± 0.01	75.01	24.98	66,921
CS-Et (NH_3^+)$_3$	65.26	81.20 ± 0.05	27.67 ± 0.01	89.52	10.48	63,631

CS-Et(NH_3^+), 76.80 Å for CS-Et(NH_3^+)$_2$, and 65.26 Å for CS-Et(NH_3^+)$_3$. This means that for the protonated systems, CS-Et(NH_3^+)$_3$ is slightly more flexible than CS-Et(NH_3^+)$_2$, which is due to the electrostatic repulsion induced by the charged amino groups. However, it must be noted that the values of persistence lengths for protonated CS are of the same order as the total length of the polymers studied (~105 Å). This indicates that the exponential fit to determine the persistence length may have a higher error. In addition, the dynamics of protonated chains may differ if the length of the polymer is not much longer than l_p. Simulations of longer protonated CS chains would be necessary, which, however, was beyond the scope of the present study.

3.3. Shift in the population of dihedral angle states

As discussed previously, two main conformational states of the CS backbone occur for the modified polymers, *syn* and *anti-ψ* (see Fig. 2(d)). The population of the *anti-φ* state is negligible (0.033 % for CS-Et(NH_2) and 0.0 % for the other systems), therefore, we do not consider it in the analyses performed. Simultaneously, it is noticeable that the states are mostly characterized by a certain ψ angle. Hence, we can simplify the visualization of the distribution of dihedral angles by plotting the probability density over ψ, see Fig. 5. There, ψ angles between −113° and 100° are considered to indicate the *syn* state, while angles outside this range can be classified as the *anti-ψ* state.

In Fig. 5(a), it is noticeable that the probability density of ψ for CS-Et(NH_2)$_2$ and CS-Et(NH_2)$_3$ differs from the one of CS-Et(NH_2), i.e. the highest peak at around −7.6° for CS-Et(NH_2) is shifted to 9.3° for CS-Et(NH_2)$_2$ and to 8.1° for CS-Et(NH_2)$_3$. Furthermore, the smaller peak at around −60° to −35° is more pronounced for CS-Et(NH_2)$_2$ and CS-Et(NH_2)$_3$. In addition, the *anti-ψ* state is more spread out for neutral CS-Et(NH_2)$_2$ than that of the other systems. This means that the range of possible angles of ψ in the *anti-ψ* state is wider. This is supported by the low persistence length and high flexibility of this polymer, as presented above. In Table 1, the population of the two mentioned states is listed for all CS systems. We can see that CS-Et(NH_2) populates mostly the *syn* state (92.29 %), while CS-Et(NH_2)$_2$ and CS-Et(NH_2)$_3$ experience a shift in population to the *anti-ψ* state and both occupy *anti-ψ* to around 25 %.

For the protonated systems, similar shifts in the *syn* state are observed (see Fig. 5(b)). This indicates that even if all polymers tend to be more fiber-like in the protonated form, the basic conformational states of dihedral angles are changed with the addition of more than one long-distanced aminated side chain. The contribution of the *anti-ψ* state is also lowered upon protonation, supporting the previous conclusion about the tendency towards more linear structures. In general, CS-Et(NH_3^+)$_2$ has the highest population of the *anti-ψ* state (14.04 %, see

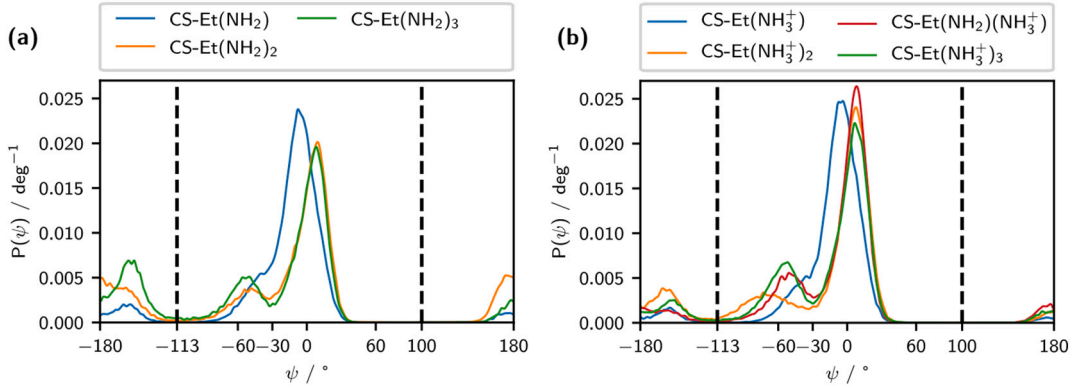

Fig. 5. Probability density of ψ dihedral angle for neutral systems (a) and protonated systems (b) calculated over 200 ns. The middle region (enclosed by vertical dashed lines) corresponds to the *syn* state, while the rest is the *anti-ψ* state.

Table 1). Yet, CS-Et(NH_3^+)$_2$ has slighly higher $\langle r_{gyr} \rangle$ than CS-Et(NH_2)(NH_3^+), by 0.49 Å.

To understand how the two states of φ and ψ dihedral angles are connected to bends in the polymer backbone, we analyzed the probability density of the linkage angle θ formed between two consecutive rings (the valence angle between atoms C1′, O4, and C4, as marked in Fig. 2(b)). θ of 180° denotes a linear linkage, resulting in a fiber-like structure of the polymer. Smaller values of this angle correspond to a bending in the backbone. The exemplary distribution of θ, plotted for neutral CS-Et(NH_2)$_2$, is depicted in Fig. S5. Two well-separated distributions of θ values are revealed: one at $\theta \approx 112°$ and one at $\theta \approx 150°$. We find that the first peak corresponds to the *anti-ψ* state, while the second one is the *syn* state. This again demonstrates that the *syn* state of CS corresponds to the rather linear geometry of the polymer backbone, whereas the *anti-ψ* state corresponds to turns in the backbone, which most probably modulate the polymer collapse. Therefore, the higher population of the *anti-ψ* state for CS-Et(NH_2)$_2$ is connected to the smaller average radius of gyration. A similar observation was captured for the other polymers considered.

3.4. Morphology modulation via intramolecular O-H···O H-bond

To understand the observed shift in conformer population towards the *anti-ψ* state in the case of CS-Et(NH_2)$_2$ and CS-Et(NH_2)$_3$ in comparison to CS-Et(NH_2) (as well as the changes between the protonated equivalents), an analysis of intramolecular hydrogen bonds (H-bonds), present during the sampling of the polymers, has been performed. All possible hydrogen bonding sites were determined and hydrogen bonds were identified for each frame of the trajectory, therefore, the calculation on 40,000 frames (200 ns) for each system was performed. We recorded H-bonds using a hydrogen-bond donor with an acceptor angle of 150° (and up to 180°, which corresponds to linear H-bonds, i.e. the most stable H-bonds). A maximum H-bond donor-acceptor distance of 3.0 Å was applied. Due to the simplicity of naming, all hydrogen bonds are named according to the atom labeling in the force field. For example, the HO3-O5 H-bond denotes an O-H···O hydrogen bond formed between the hydrogen atom bonded to the O3 atom and the O acceptor labeled as O5. Atom labeling used for all repeat units is depicted in Figs. S7-S9. The HO3-O5 H-bond is marked in Fig. 2(b) with a dashed red line.

To assign the role of the particular hydrogen bond in attaining the conformational state of CS (*syn/anti-ψ*), for each hydrogen bond between neighboring monosaccharide units, we determined the dihedral angle ψ formed between the two repeat units, as depicted in Fig. 2(a). Several types of possible H-bond donors and acceptors, forming the most populated H-bonds, were identified. Since the contribution of the hydrogen bond between HO3 and O5 (see Fig. 2(b)) was found to be the strongest, we have first conducted its analysis. In Table 1, the total number of HO3-O5 H-bonds for every system is listed. For CS-Et(NH_2), around 230,000 H-bonds were found. This means that there are an average of about six HO3-O5 H-bonds per frame in MD. Also, these hydrogen bonds are all formed in the *syn* dihedral state, which is a more linear conformation of the polymer backbone, allowing for stable intramolecular H-bonding (see Fig. 2(b)). For comparison, a linkage in the *anti-ψ* state is depicted in Fig. 2(c). Due to the rotation of the hydroxy group containing the HO3 hydrogen atom away from the accepting oxygen O5, the mentioned H-bond cannot be formed in the *anti-ψ* state. Similar dependence was reported by Tsai et al. [29].

For CS-Et(NH_2)$_2$/CS-Et(NH_2)(NH_3^+)/CS-Et(NH_3^+)$_2$ and CS-Et(NH_2)$_3$/CS-Et(NH_3^+)$_3$, the HO3 atom of chitosan is replaced by a long-distanced aminated modification. Therefore, no HO3-O5 hydrogen bonds can be formed between the CS units. However, there are still unmodified chitin units (GlcNAc) in the systems due to the simulated 80 % DD. Therefore, the HO3-O5 H-bonds measured originate from the interactions between GlcNAc (chitin) and GlcN (modified CS) units. This is why there are fewer detected H-bonds, around 67,000 to 74,000 for CS-Et(NH_2)$_3$ and CS-Et(NH_2)$_2$, respectively. The significant decrease in the HO3-O5 hydrogen bonds from CS-Et(NH_2) to CS-Et(NH_2)$_2$/CS-Et(NH_2)$_3$ is one of the major reasons for the shift in the population of conformational states from the *syn* state to the *anti-ψ* state. This also explains the smaller average radius of gyration for CS-Et(NH_2)$_2$ and CS-Et(NH_2)$_3$ (see Fig. 4 (a)) in comparison to CS-Et(NH_2): there are fewer stabilizing HO3-O5 H-bonds, and therefore, more backbone turns (especially between modified CS units). In addition, due to other interactions between the side chains, a more pronounced collapse of the backbone is caused.

If we compare only the HO3-O5 H-bonds formed between modified CS units of the polymers and unmodified chitin units, 96,174, 73,804, and 66,921 H-bonds are formed for CS-Et(NH_2), CS-Et(NH_2)$_2$, and CS-Et(NH_2)$_3$, respectively. The difference between the last two is much smaller and, in general, fewer H-bonds close to the polymer backbone exist. This explains why CS-Et(NH_2)$_2$ and CS-Et(NH_2)$_3$ have a very similar population of the *anti-ψ* state (~25 %, see Table 1). However, this does not explain why the CS-Et(NH_2)$_2$ chain is more flexible than CS-Et(NH_2)$_3$ and forms more dense coils. The only structural difference between CS-Et(NH_2)$_2$ and CS-Et(NH_2)$_3$ is that CS-Et(NH_2)$_2$ still has an unmodified amino group of chitosan (Fig. 1), while for CS-Et(NH_2)$_3$ this amino group is replaced with a long side chain ending in an amino group. We looked at hydrogen bonds formed at the sites in which CS-Et(NH_2)$_2$ and CS-Et(NH_2)$_3$ differ and no significant differences were observed (see Table S2). This indicates the possibility of other interactions close to the backbone to modulate this change, e.g. with water molecules. Furthermore, different patterns of H-bond interactions between the side chains may also occur and change the dynamics of both polymers and their collapsing propensity. In addition, the lower flexibility and higher average radius of gyration of CS-Et(NH_2)$_3$ may come from the steric effects of the additional side chain, hindering dense collapse with highly packed side groups. This may also be the reason why the *anti-ψ* state of CS-Et(NH_2)$_3$ is not as wide (and the polymer thus is less flexible) as the one of CS-Et(NH_2)$_2$ (Fig. 5(a)).

For the protonated systems, the number of HO3-O5 hydrogen bonds is similar to those of the neutral systems. This is reasonable since only the amino groups are protonated and they do not directly participate in the HO3-O5 formation close to the backbone. It stands out, however, that protonation induces more significant changes in the case of CS-Et(NH_2)$_2$. The protonation of the long-distanced chains (CS-Et(NH_2)(NH_3^+)) results in the change of the HO3-O5 H-bonds (between chitin and CS units) from 73,804 to 62,009, higher linearization of the polymer chain, and a shift towards the *syn* state (Table 1). However, this number drops significantly in the case of the additional protonation of the amino group near the backbone (CS-Et(NH_3^+)$_2$) and only 35,540 HO3-O5 hydrogen bonds were counted. This is a clear sign that the role of this group in the dynamics of the polymer with two long-distanced side chains is essential.

3.5. Interplay of noncovalent interactions towards polymer collapse

The formation of the previously described HO3-O5 H-bond is the most characteristic of the polymers studied due to the chitosan-based backbone. However, the derivatization of CS modulates the possibility of other H-bond formation, which may contribute to its structural changes in water. The total number of recorded H-bonds, without counting the dominating HO3-O5 H-bonds, is 28,726, 20,132, and 19,002 for CS-Et(NH_2), CS-Et(NH_2)$_2$, and CS-Et(NH_2)$_3$, and 30,447, 23,473, 43,466, and 31,760 for CS-Et(NH_3^+), CS-Et(NH_2)(NH_3^+), CS-Et(NH_3^+)$_2$, and CS-Et(NH_3^+)$_3$, respectively. CS-Et(NH_2) is not too packed by the presence of side chain modifications and tends to be in the *syn* state (Figs. 4 and 5), therefore, more H-bonds, e.g. involving the HO6 donor (see Fig. S7), could be formed during 200 ns MD. The difference in H-bond formation between CS-Et(NH_2)$_2$ and CS-Et(NH_2)$_3$ is rather negligible, especially considering the fact that the addition of the third side chain modification could, in principle, introduce a higher possibility of H-bonds being formed.

For the estimation of the role of intramolecular H-bonds on the

conformation of CS and the change upon protonation, we have focused on the analysis of CS-Et(NH_2) and CS-Et(NH_3^+). The summary of the most populated H-bond donors and acceptors and their contribution to the *syn* and *anti-ψ* states are given in Fig. 6. It can be revealed that the *syn* state is stabilized mainly by HO3-O5, HO6-N1, HO6-N2, HO6-O3, and HO3-O6 H-bonds. Other sets of H-bonds occur in the *anti-ψ* state, e.g., HO6-O5, HO6-O6, and HO3-N1.

The protonation of CS-Et(NH_2) reduces the possibility of the formation of some H-bonds while increasing the content of others. The most significant change occurs for HO6-N2, HO6-O6, HO3-N2, and HO3-O6, as well as the already discussed HO3-O5 H-bond. All of them are less likely to occur. In comparison, the amount of HO6-N1 H-bonds slightly increases. A similar analysis could not be performed for the other polymers due to the significantly higher possibility of diverse H-bonds with rather small contributions, i.e. on average, with lower lifetimes and only a temporary impact on the conformational states.

To estimate H-bonds formation considering distant repeat units, for each hydrogen bond we define Δn as the number of linkages between the monomer, containing the H-bond acceptor, and the monomer, containing the H-bond donor. Hence, $\Delta n = 0$ means that the donor and acceptor belong to the same repeat unit of CS. If $\Delta n = 1$, the H-bond donor originates from the first neighboring repeat unit of the acceptor, and so on. The summary of the intramolecular H-bonds, excluding the dominating HO3-O5 H-bonds, captured for repeat units up to the sixth neighbor, is given in Table 2.

We notice that most hydrogen bonds formed during MD of the polymers in neutral and protonated states originate from interactions within the repeat unit and up to $\Delta n = 1$. The formation of H-bonds with $\Delta n = 2$ is < 10.00 % for all forms except protonated CS-Et(NH_3^+)$_3$ with 18.24 %. The impact of H-bonds with $\Delta n = 2$ is the lowest for neutral CS-Et(NH_2) (3.22 %) because the interacting side chains are rather well separated and the polymer tends to be in the *syn* state. The repulsive interactions due to protonation lower the possibility of H-bond formation for $\Delta n < 2$, therefore, the formation of intramolecular H-bonds is slightly shifted towards $\Delta n = 2$.

For repeat units with $\Delta n > 2$, the formation of H-bonds is pronounced only for the neutral CS-Et(NH_2)$_2$. Here, H-bonds with the third neighboring repeat unit amount to 4.81 %. This indicates that the chemical composition of the polymer permits interactions between the side chains and this may be the reason for the densely packed collapse patterns and lower radius of gyration in comparison to the other CS modifications. The visualization of some exemplary snapshots of CS-Et(NH_2)$_2$ with occurring H-bonds, as well as the noncovalent interaction (NCI) surfaces, are demonstrated in Fig. 7. If an attractive interaction between atoms occurs, the position of the interaction is marked by green surfaces

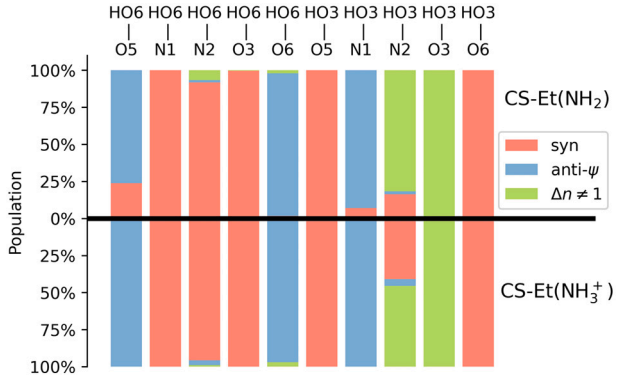

Fig. 6. The most populated intramolecular hydrogen bonds in CS-Et(NH_2) and CS-Et(NH_3^+) recorded over 200 ns. The percentages indicate the fraction of the respective hydrogen bonds formed in the *syn* and *anti-ψ* conformation. Atom labels are provided in Fig. S7, while all values (including the absolute number of occurrences) are listed in Table S3 for clarity.

(see the description of the NCI analysis in SI). The selected N-H···O H-bonds between the side chain and the backbone and between the two side chains with the length of 2.43 Å and 2.54 Å are marked in Fig. 7(a), respectively. An O-H···O H-bond, stabilizing the temporary *syn* state, is marked in Fig. 7(b) with the length of 1.75 Å. One N-H···N and two N-H···O H-bonds are marked with the H-bond lengths of 2.80 Å, 2.28 Å, and 2.27 Å, respectively. During the analysis of the NCI surfaces (marked in green in Fig. 7), we noticed the existence of weak C-H···O and C-H···N H-bonds, which were not considered in the analysis of MD simulations. Moreover, a significant contribution of van der Waals interactions has been detected. The qualitative analysis of the type and strength of the NCI is given in Fig. S10.

The protonation of the side chains of CS-Et(NH_2)$_2$ (CS-Et(NH_2)(NH_3^+) polymer) decreases H-bonds with the third neighboring repeat unit from 4.81 % to 1.76 % (see Table 2). At the same time, the contribution of H-bonds between the neighboring units ($\Delta n = 1$) increases from 78.38 % to 86.48 %. The complete protonation of this polymer (CS-Et(NH_3^+)$_2$ polymer), which adds the additional repulsion close to the polymer backbone (via the amino group), changes the H-bonding pattern, i.e. the relative contribution of H-bonds for $\Delta n = 1$ decreases to 55.79 %, while for $\Delta n = 0$ it increases from 3.67 % - 7.14 % to 36.60 %. This observation indicates that the protonation of the amino group close to the polymer backbone has a strong impact on hindering polymer collapse and yields further linearization, e.g. towards increased solubility. Due to the fact that this group is located more inside the polymer and may be less accessible to the solvent, the experimental conditions may be closer to polymer characteristics of CS-Et(NH_2)$_2$ and CS-Et(NH_2)(NH_3^+) states, explaining the increased collapse found in experiment [15,47]. Therefore, the protonation of this amino group, i.e. full protonation, would be necessary to increase the surface area of CS with two modified side chains. However, it may be suppressed due to possible pK_a decrease of CS-Et(NH_2)$_2$, resulting in a higher content of neutral CS units at the same pH conditions.

To understand the impact of the chitin units in the polymer backbone and the possibility of intramolecular H-bonds between pairs of CS-modified repeat units (GlcN-GlcN) and CS-modified units with chitin (GlcN-GlcNAc), the occurrence of H-bonds in both types of linkages was analyzed. The results are listed in Table S4, where we excluded the dominating HO3-O5 hydrogen bonds. A significantly higher amount of H-bonds is seen between modified CS units and chitin units for polymers with two and three long-distanced side chains. Around 15,000 of such H-bonds were captured for neutral CS-Et(NH_2)$_2$ and CS-Et(NH_2)$_3$, while CS-Et(NH_2) has only approximately half of that. A similar observation is valid for the protonated systems as well. This may also impact the population of the *syn* and *anti-ψ* states and, together with the missing HO3 H-bond donor, may be the reason for more similarities between the conformational states of CS-Et(NH_2)$_2$ and CS-Et(NH_2)$_3$ in comparison to CS-Et(NH_2).

Finally, after the analysis of each particular H-bond occurring > 100 times during MD, we noticed that CS-Et(NH_2)$_2$, in comparison to CS-Et(NH_2)$_3$, is stabilized by the neighboring ($\Delta n = 1$) HO6-O3 and HO6-O6 H-bonds, as well as HO6-N6 and HO6-N5 H-bonds with $\Delta n = 3$ (atom labels are depicted in Figs. S7, S8). They include the HO6 H-bond donor from chitin units. This means that the CS-Et(NH_2)$_2$ structure tends to be more sensitive to the presence of the chitin units. In addition, the contribution of H56-O6 and H55-O6 H-bonds ($\Delta n = 1$), involving the amino group, is also noticeable.

3.6. Polymer-water interactions

Crosslinked chitosan is generally used as a pH-sensitive hydrogel and its swellability in water is mainly driven by electrostatic interactions induced upon polymer protonation, which decrease the polymer aggregation propensity [27,30]. It was reported that pristine and aminated CS (with one and three aminated side chains, i.e. CS-Et(NH_2) and CS-Et(NH_2)$_3$, respectively) show similar thermal decomposition and content

Table 2
Number of intramolecular hydrogen bonds in modified CS polymers and their contribution (in % with respect to the total number of H-bonds). H-bonds between repeat units with distance up to $\Delta n = 6$ are listed. The dominating HO3-O5 H-bonds for $\Delta n = 1$ were not considered in this table.

System	Δn							
	0	1	2	3	4	5	6	Total
CS-Et(NH_2)	3082	24,088	926	74	9	4	142	28,726
	10.73 %	83.85 %	3.22 %	0.26 %	0.03 %	0.01 %	0.49 %	
CS-Et(NH_3^+)	3730	24,269	2367	70	11	0	0	30,447
	12.25 %	79.71 %	7.77 %	0.23 %	0.04 %	0.00 %	0.00 %	
CS-Et(NH_2)$_2$	1437	15,779	1764	968	115	19	23	20,132
	7.14 %	78.38 %	8.76 %	4.81 %	0.57 %	0.09 %	0.11 %	
CS-Et(NH_2)(NH_3^+)	862	20,299	1878	412	20	2	0	23,473
	3.67 %	86.48 %	8.00 %	1.76 %	0.09 %	0.01 %	0.00 %	
CS-Et(NH_3^+)$_2$	15,910	24,251	3052	249	4	0	0	43,466
	36.60 %	55.79 %	7.02 %	0.57 %	0.01 %	0.00 %	0.00 %	
CS-Et(NH_2)$_3$	1627	15,052	1888	333	67	27	4	19,002
	8.56 %	79.21 %	9.94 %	1.75 %	0.35 %	0.14 %	0.02 %	
CS-Et(NH_3^+)$_3$	3213	22,377	5794	373	2	1	0	31,760
	10.12 %	70.46 %	18.24 %	1.17 %	0.01 %	0.00 %	0.00 %	

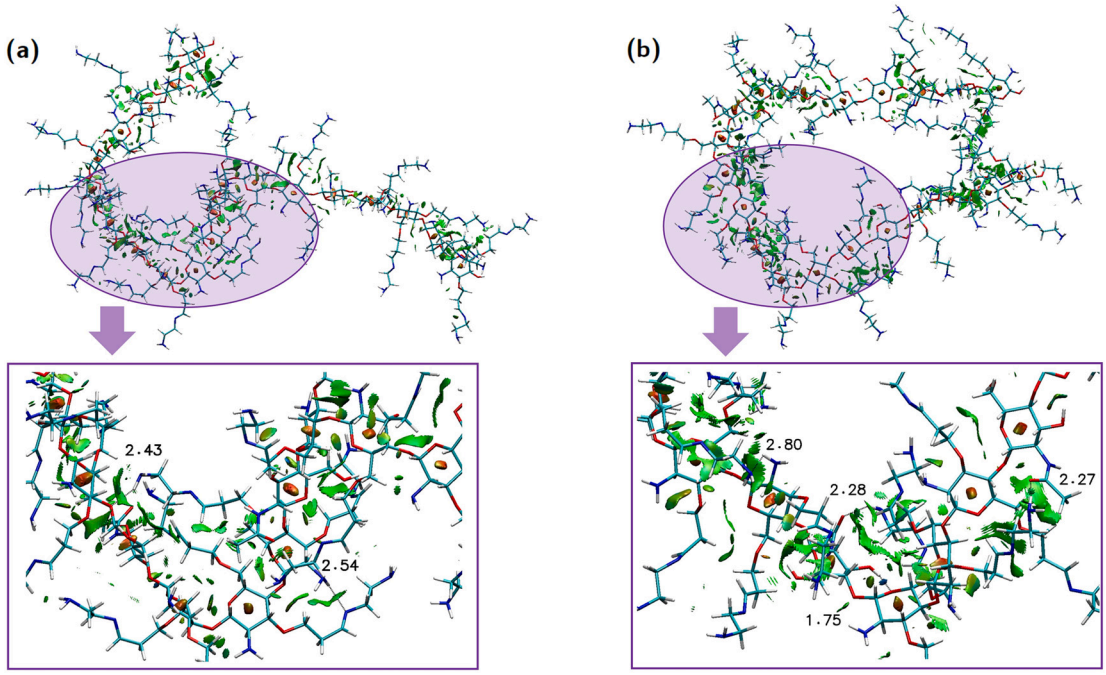

Fig. 7. Two exemplary snapshots of the CS-Et(NH_2)$_2$ polymer, demonstrating intramolecular noncovalent interactions in the polymer. Both van der Waals interactions and H-bonding are marked by green surfaces. They correspond to the reduced density gradient (s) of 0.3 a.u. (see SI). The color scale of the density of $-0.04 < \rho < 0.04$ a.u. was used for the visualization. The zoomed region of the polymer is indicated by the purple area. The selected H-bonds, N-H···O/N-H···N (a) and N-H···N/O-H···O/two N-H···O (b) with the H-bond lengths of 2.43 Å/2.54 Å and 2.80 Å/1.75 Å/2.27–2.28 Å, respectively, are marked.

of water during the thermogravimetric analysis of the polymers in nitrogen and in air [47]. CS with two modified side chains (CS-Et(NH_2)$_2$) demonstrated a diverse behavior. It possessed a much higher water content, which was released in several stages of thermal degradation, and it was more stable during thermal degradation. From the analysis of the polymer structural dynamics and intramolecular H-bonding, we also observe differing characteristics of CS-Et(NH_2)$_2$, especially for its neutral form. Moreover, higher collapse and the possibility of interactions between several side chains were captured, therefore, there is evidence for the formation of densely packed collapsed structures. To understand the differences in the water binding of all considered CS systems, a detailed analysis of H-bonds and polymer-water binding modes has been performed.

All chitosans studied show the same types of H-bonds formed with water. Polymers play the role of H-bond acceptors with N and O atoms as the contributing players. Here, N2 (similarly to N6), N4, O3, and O6 are the most common H-bond acceptors participating in the binding of water. There are also H-bond donors enabled by amino groups. We used H13 and H45 as examples contributing to H-bonds as donating parts. The contribution of each of the H-bond types is listed in Table 3.

Considering the higher amount of hydrogen atoms in the protonated forms of the CS polymers, there are more possible H-bonds to be formed. This is clearly visible from the probability distribution of the number of formed H-bonds, visualized in Fig. 8. In Table 3, only one type of hydrogen atom per modification, e.g. H13, present in the side chain of CS-Et(NH_2), and H45, belonging to the modification near the O3 atom of CS-Et(NH_2)$_2$ and CS-Et(NH_2)$_3$ (see Figs. S7-S9), is given. Their absolute contributions (Table S5) can be multiplied by the number of active hydrogen atoms in the amino group to get the complete contribution of aminated side chains in the formation of H-bonds with water. In the case of semiprotonated CS-Et(NH_2)(NH_3^+) and protonated CS-Et(NH_3^+)$_2$, the contribution of aminated side chains is dominant among all H-bonds

Table 3
Occurrences of the most populated hydrogen bonds between CS polymers and water recorded over 200 ns and given as the %-contribution with respect to the total number of H-bonds with water recorded for the respective system (absolute numbers are given in Table S5). Hydrogen bonds are labeled using the atom names given in Figs. S7, S9. The oxygen atom of water is labeled as O_w, while the hydrogen atom of water is labeled as H_w.

	N2 – H_w	N4 - H_w	O6 - H_w	O3 - H_w	H13 - O_w	H45 - O_w
	Occurrence of H-bonds / %					
CS-Et(NH_2)	18.66	–	17.04	14.98	0.32	–
CS-Et(NH_3^+)	6.07	–	14.57	13.16	10.73	–
CS-Et(NH_2)$_2$	–	18.06	11.47	11.04	–	0.33
CS-Et(NH_2)(NH_3^+)	–	4.65	9.12	8.90	–	9.30
CS-Et(NH_3^+)$_2$	–	3.72	5.66	3.36	–	8.24
CS-Et(NH_2)$_3$	14.29	13.75	8.39	8.22	0.26	0.26
CS-Et(NH_3^+)$_3$	–	3.44	5.65	6.06	6.93	6.89

formed between CS and water. Since the protonation of the long-distanced side chains for these two polymers is the same, the solvent-accessible surface area (SASA) is rather similar (see Fig. S15).

The neutral forms of CS possess negligible content of water bonded by H-bonds to NH_2 groups, 0.32 % and 0.26 % of H13-O_w for CS-Et(NH_2) and CS-Et(NH_2)$_3$ were counted, respectively. However, higher content of N2-H_w and N4-H_w of around 14 % to 18 % occurs, while it decreases to 3 %–6 % after protonation (see Table 3). The change in the content of O6-H_w and O3-H_w is lower, and it is more pronounced for the CS-Et(NH_2)$_2$ polymer, especially after the protonation of the NH_2 group close to the backbone (CS-Et(NH_3^+)$_2$). Interestingly, the total amount of H-bonds detected for CS-Et(NH_2) and CS-Et(NH_2)$_2$ is rather similar (see Fig. 8(a)), however, CS-Et(NH_2)$_2$ contains more H-bond acceptors than CS-Et(NH_2). The SASA is also increased not proportionally (depicted in Fig. S14). This is most probably related to the higher collapse of CS-Et(NH_2)$_2$, explained above. Moreover, the lifetime of some H-bonds formed between CS-Et(NH_2)$_2$ and water is longer than in the case of CS-Et(NH_2), e.g., the lifetime of O6-H_w and O3-H_w is 7.77 ps and 6.53 ps for CS-Et(NH_2)$_2$, and 3.64 ps and 4.80 ps for CS-Et(NH_2). The H-bond lifetimes are listed in Table S6. Rather small differences in the decrease of lifetimes of these H-bonds are noticeable after polymer protonation.

An increase in the lifetime of O3-H_w was detected for semi-protonated CS-Et(NH_2)(NH_3^+), from 6.53 ps to 8.13 ps, with a subsequent decrease to 4.57 ps for protonated CS-Et(NH_3^+)$_2$. Since this H-bond occurs close to the NH_2 near the backbone, we assume that H-bonds networking patterns between the polymer and water may take place, inducing a higher water bonding capacity of this polymer. Since only CS-Et(NH_2)$_2$ possesses one unmodified amino group from pure chitosan, it behaves differently from the other polymers considered.

3.7. Beyond the bound water

Water in hydrogels can be classified into several types, including bound, intermediate, and free water [55,56]. The specific contribution of each water type impacts the water structuring around the polymer, and therefore, the polymer biocompatibility and binding of adsorbates. Bound water interacts with a polymer by forming H-bonds with its hydrophilic groups, and therefore, it is close to the polymer. A distance of 2.8 Å between the oxygen of bound water and the carbonyl oxygen of poly-*N*,*N*-dimethylacrylamide has been reported previously [55]. Intermediate water forms H-bonds with the bound water. It does not directly interact with the polymer, but it is involved in networking within the hydration shell. Therefore, O-O distances were found to be slightly larger, e.g. from 4.5 Å up to 5.3 Å. Water molecules that are free of any interactions involving the polymers are defined as free water.

Since the classification of the water types is mostly based on distance criteria, we calculated the radial distribution function (RDF) of distances between N (and O) atoms from the CS polymers and O atoms belonging to water. This is depicted in Figs. 9 and S13. Peaks of N-O_w distances can be found at 2.7 Å, 4.7 Å, and 7.5 Å for the neutral forms of CS and at 2.9 Å, 4.9 Å, and 7.7 Å for the protonated polymers. CS-Et(NH_2) and CS-Et(NH_2)$_3$ show similar contributions of bound water, while CS-Et(NH_2)$_2$ has a slightly lower amount. Moreover, CS-Et(NH_2) has more intermediate and free water. This may be explained both by the less packed structure of CS-Et(NH_2), enabling intermediate water molecules to interact better with bound water near the polymer, and by the presence of the HO3 atom in CS-Et(NH_2), allowing for better water networking around the unmodified group. The contribution of all three mentioned water types is nearly equal in the case of CS-Et(NH_2), while it gradually decreases for CS-Et(NH_2)$_3$. CS-Et(NH_2)$_2$ demonstrates a smaller probability of direct binding of water molecules, e.g., the intensity of the first peak is slightly lower than for CS-Et(NH_2) and CS-Et(NH_2)$_3$ and water distances to the polymer are more spread out (see the inset in Fig. 9(a)). This can be explained by the higher collapsing propensity of CS-Et(NH_2)$_2$. However, it binds significantly more water at the minimum located at the N-O_w distance of 3.7 Å, which is shifted by 0.2 Å compared to the other polymers. We assume this originates from the orientation of water molecules around the amino group near the backbone since it is harder to orient in the confinement space between other flexible long-distanced side chains. Moreover, we have captured some H-bonds between these NH_2 groups (atom N8) and water for CS-Et(NH_2)$_2$ (3877 H-bonds) and CS-Et(NH_2)(NH_3^+) (4376 H-bonds). We also see that the intensity of intermediate water is slightly higher than that of the bound water in this case (the second peak in Fig. 9(a) is higher than the first one).

Much more bound water is characteristic for the protonated CS-Et(NH_3^+)$_2$ (in orange in Fig. 9(b)) in comparison to the neutral form. This is directly connected to the shift from the *anti-ψ* to the *syn* state and the

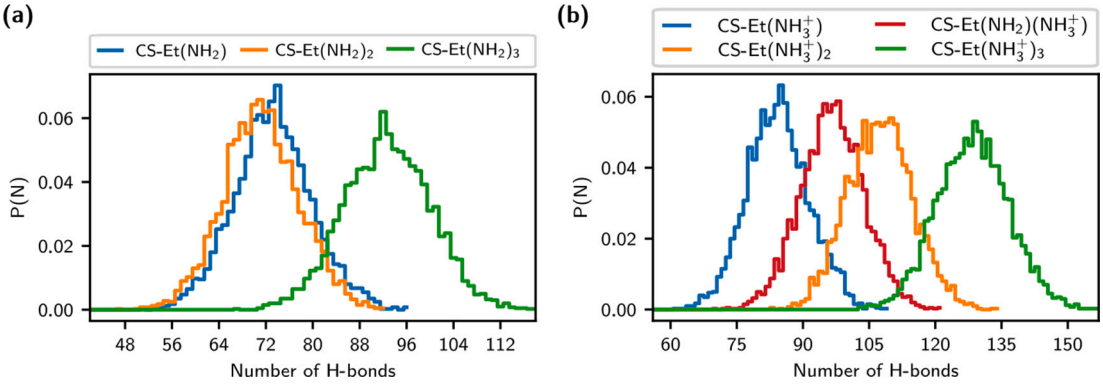

Fig. 8. Number of hydrogen bonds formed between modified CS and water molecules, (a) for the neutral forms, (b) for the protonated forms. The time evolution of the H-bonds formed during 200 ns of MD is depicted in Figs. S11 and S12.

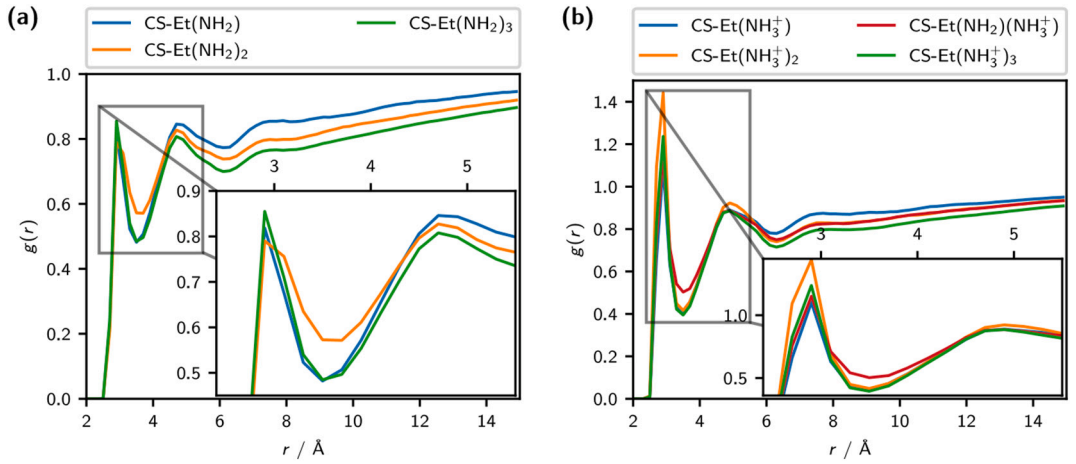

Fig. 9. The radial distribution function for the distances between the nitrogen atoms of the polymers and the oxygen atoms of water, (a) for the neutral systems, (b) for the protonated systems.

polymer linearization modulated by repulsion interactions. The amount of intermediate water (the second peak, at 4.9 Å) is also the highest among all polymers studied. Furthermore, clear evidence of the essential role of NH_2 of CS-Et$(NH_3^+)_2$ (close to the backbone) and its protonation on the polymer water binding can be observed. For CS-Et$(NH_2)(NH_3^+)$, the amount of water at the N-O_w distances of 3.5 Å deviates, similarly, as for the neutral CS-Et$(NH_2)_2$. As stated above, evidence for H-bond formation between the NH_2 group close to the backbone and water was detected. Therefore, the lack of protonation of this amino group partially shifts the content of bound water (the first peak in Fig. 9(b)) towards weakly bound water with N-O_w distances around 3.5 Å. There are no significant differences between other water types for CS-Et(NH_3^+), CS-Et $(NH_2)(NH_3^+)$, and CS-Et$(NH_3^+)_3$.

The distinguishing content of intermediate water can also be demonstrated by the RDF of oxygen-oxygen distances, i.e. between oxygen atoms of CS and oxygen atoms of water (see Fig. S13). The second peak of the CS-Et$(NH_2)_2$ polymer (in all states studied) is more populated and the polymer does not follow the trends of the other systems. Here, CS-Et(NH_2) and CS-Et(NH_3^+) show much more bound water than the other polymers, because only here the hydroxy group (HO3 atom) was not modified, thus, closer distances of water to the polymer are allowed.

A visible increase in the hydrophilicity of CS polymers after protonation is noticeable in all cases studied. The probability of bound waters located in the polymer's close vicinity is drastically shifted towards direct binding via H-bonding. The same dependence has been observed by the analysis of H-bonds, as stated before.

4. Discussion

MD simulations of the aminated chitosans and diverse analyses of their intra- and intermolecular interactions allowed us to get more insights into the behavior of three different CS derivatives. We clearly see the deviating characteristics of the polymer with two modified side chains, which is in line with the reported performance of the polymers in experiments [15,47].

We demonstrate that the conformational states of CS explicitly depend on the intramolecular H-bond patterns. Moreover, the type of modification introduced is shown to change the population of the dihedral angle conformations. The substitution of the HO3 atom of pristine CS disables the formation of the key intramolecular HO3-O5 H-bond and thus induces twists and turns within the polymer backbone, causing a higher population of the *anti-ψ* conformational state and a higher tendency towards collapse. This may impact the surface area of the polymer and its possibility for adsorbate binding, as was reported experimentally for the CS modified with two long-distanced side chains: it binds the least amount of human serum albumin in comparison to the other two CS derivatives [15]. In the present study, from the analysis of the polymer radius of gyration, persistence length, and end-to-end distance, evidence towards a more significant collapse of this polymer is revealed.

With the in-depth analysis of diverse H-bonding patterns, modulating polymer structure formation, we found that the modification of the amino group near the polymer backbone (present in pristine chitosan) could be essential in hindering polymer collapse. At the same time, both intramolecular H-bonds, partially depending on the degree of deacetylation, and intermolecular H-bonds with water are shown to be steered by the presence of this amino group. We demonstrate that specific binding of water molecules, especially the intermediate water, is more pronounced in the polymer with such an amino group, i.e. CS-Et $(NH_2)_2$. Moreover, from the behavior of this polymer in water, we assume it should possess a more irregular and complex surface morphology compared to the other more linearized systems studied. This could also contribute to increased water binding capacity by providing more surface sites for water adsorption. Together with the higher tendency towards collapse of CS-Et$(NH_2)_2$ (as well as its semi-protonated form CS-Et$(NH_2)(NH_3^+)$) and locking of water inside of the polymer, we believe this is a possible explanation for the higher water binding and higher water content of this type of modified CS.

The change in the properties of the polymers upon the change of pH, i.e. after protonation, could also be revealed by the simulations performed. Higher linearization, i.e. the fiber-like structure of the polymers, is clearly visible as a result of repulsion interactions. An increase in water binding and a change in the type of water around the polymers are shown. In addition, we found a shift towards a higher content of bound water after the protonation and explain, in detail, the change in the intermolecular H-bond pattern. Moreover, the analysis of intramolecular H-bonds is shown to indicate a change in the conformational states of the modified CS.

It should be noted that the present investigation, performed on a representative fragment of three different chitosan polymers, brings new insights into the understanding of the properties of polymers obtained experimentally. However, longer polymer chains, with diverse degrees of derivatization, as well as the behavior of several chains simulated for a longer time, may need to be analyzed to reveal other macroscopic phenomena, such as polymer aggregation or immobilization of biological macromolecules.

Finally, we hope this study demonstrates the importance of the computational investigation of chitosan derivatives (as well as other polymers) and the increased tendency towards the virtual design and

pre-screening of diverse side chain modifications yielding the desired functionality of the polymers.

5. Conclusions

To understand the differences in the properties of modified chitosan derivatives, MD simulations with an adapted parameterization scheme using the combination of the CHARMM force field for carbohydrates and the CHARMM General Force Field were performed. The conformational analysis of the polymers and the analysis of the diverse set of interactions, with a special focus on H-bond formation, have been performed. Evidence of differences among the polymers and the explanation of previously reported experimental observations were provided. The impact of the type of amination on polymer dynamics and possible performance was discussed.

Funding sources

Authors acknowledge funding from the Deutsche Forschungsgemeinschaft (DFG) via the GRK 2450 "Scale bridging methods of computational nanoscience". MK acknowledges funding from the Ministry of Science, Research and Art Baden-Württemberg (Germany) under Brigitte-Schlieben-Lange-Programm. Authors acknowledge support by the KIT-Publication Fund of the Karlsruhe Institute of Technology.

CRediT authorship contribution statement

Henrik Schopmans: Writing – review & editing, Writing – original draft, Visualization, Validation, Software, Methodology, Investigation, Formal analysis, Data curation, Conceptualization. **Tillmann Utesch:** Writing – review & editing, Methodology. **Patrick Théato:** Writing – review & editing, Conceptualization. **Maria Andrea Mroginski:** Writing – review & editing, Resources, Methodology. **Mariana Kozlowska:** Writing – review & editing, Writing – original draft, Visualization, Validation, Supervision, Software, Resources, Project administration, Methodology, Investigation, Funding acquisition, Formal analysis, Conceptualization.

Declaration of competing interest

The authors declare no conflict of interest.

Appendix A. Supplementary data

Parameterization setup of the aminated chitosans, as well as additional analyses of structural parameters of the macromolecules are available in Supplementary data to this article at https://doi.org/10.1016/j.ijbiomac.2024.136159, as well as under https://doi.org/10.17172/NOMAD/2024.05.31-1.

References

[1] V.K. Thakur, S.I. Voicu, Recent advances in cellulose and chitosan based membranes for water purification: a concise review, Carbohydr. Polym. 146 (2016) 148–165, https://doi.org/10.1016/j.carbpol.2016.03.030.
[2] G.A.F. Roberts, Chitin Chemistry, Macmillan, 1992.
[3] R.A. Cunha, T.A. Soares, V.H. Rusu, F.J.S. Pontes, E.F. Franca, R.D. Lins, The molecular structure and conformational dynamics of chitosan polymers: an integrated perspective from experiments and computational simulations, in: The Complex World of Polysaccharides, Oct. 2012, https://doi.org/10.5772/51803.
[4] P. Miretzky, A.F. Cirelli, Hg(II) removal from water by chitosan and chitosan derivatives: a review, J. Hazard. Mater. 167 (1) (2009) 10–23, https://doi.org/10.1016/j.jhazmat.2009.01.060.
[5] P.O. Boamah, Y. Huang, M. Hua, Q. Zhang, J. Wu, J. Onumah, L.K. Sam-Amoah, P. O. Boamah, Sorption of heavy metal ions onto carboxylate chitosan derivatives—a mini-review, Ecotoxicol. Environ. Saf. 116 (2015) 113–120, https://doi.org/10.1016/j.ecoenv.2015.01.012.
[6] B.G. Fouda-Mbanga, E. Prabakaran, K. Pillay, Carbohydrate biopolymers, lignin based adsorbents for removal of heavy metals (Cd2+, Pb2+, Zn2+) from wastewater, regeneration and reuse for spent adsorbents including latent fingerprint detection: a review, Biotechnol. Rep. 30 (2021) e00609, https://doi.org/10.1016/j.btre.2021.e00609.
[7] S. Zhang, Y. Dong, Z. Yang, W. Yang, J. Wu, C. Dong, Adsorption of pharmaceuticals on chitosan-based magnetic composite particles with core-brush topology, Chem. Eng. J. 304 (2016) 325–334, https://doi.org/10.1016/j.cej.2016.06.087.
[8] N. Aramesh, A.R. Bagheri, M. Bilal, Chitosan-based hybrid materials for adsorptive removal of dyes and underlying interaction mechanisms, Int. J. Biol. Macromol. 183 (2021) 399–422, https://doi.org/10.1016/j.ijbiomac.2021.04.158.
[9] Z. Moridi mahdieh, V. Mottaghitalab, A. Haghi, A detailed review of recent progress in carbon nanotube/chitosan nanocomposites, Cellul. Chem. Technol. 45 (2011) 549–563.
[10] V. Mani, M. Govindasamy, S.-M. Chen, T.-W. Chen, A.S. Kumar, S.-T. Huang, Core-shell heterostructured multiwalled carbon nanotubes@reduced graphene oxide nanoribbons/chitosan, a robust nanobiocomposite for enzymatic biosensing of hydrogen peroxide and nitrite, Sci. Rep. 7 (1) (2017) 11910, https://doi.org/10.1038/s41598-017-12050-x.
[11] S.K. Shukla, A.K. Mishra, O.A. Arotiba, B.B. Mamba, Chitosanbased nanomaterials: a state-of-the-art review, Int. J. Biol. Macromol. 59 (2013) 46–58, https://doi.org/10.1016/j.ijbiomac.2013.04.043.
[12] S. Peers, A. Montembault, C. Ladavière, Chitosan hydrogels for sustained drug delivery, J. Control. Release 326 (2020) 150–163, https://doi.org/10.1016/j.jconrel.2020.06.012.
[13] M. Dash, F. Chiellini, R. Ottenbrite, E. Chiellini, Chitosan — a versatile semi-synthetic polymer in biomedical applications, Prog. Polym. Sci. 36 (2011) 981–1014, https://doi.org/10.1016/j.progpolymsci.2011.02.001.
[14] T. Kean, M. Thanou, Biodegradation, biodistribution and toxicity of chitosan, Adv. Drug Deliv. Rev. 62 (1) (2010) 3–11, https://doi.org/10.1016/j.addr.2009.09.004.
[15] M. Ziegler-Borowska, K. Mylkie, M. Kozlowska, P. Nowak, D. Chelminiak-Dudkiewicz, A. Kozakiewicz, A. Ilnicka, A. KaczmarekKedziera, Effect of geometrical structure, drying, and synthetic method on aminated chitosan-coated magnetic nanoparticles utility for HSA effective immobilization, Molecules 24 (10) (2019) 1925, https://doi.org/10.3390/molecules24101925.
[16] F. Ding, H. Deng, Y. Du, X. Shi, Q. Wang, Emerging chitin and chitosan nanofibrous materials for biomedical applications, Nanoscale 6 (16) (2014) 9477–9493, https://doi.org/10.1039/C4NR02814G.
[17] Y. Gao, Y. Wu, Recent advances of chitosan-based nanoparticles for biomedical and biotechnological applications, Int. J. Biol. Macromol. 203 (2022) 379–388, https://doi.org/10.1016/j.ijbiomac.2022.01.162.
[18] M. Taghizadeh, A. Taghizadeh, M.K. Yazdi, P. Zarrintaj, F.J. Stadler, J.D. Ramsey, S. Habibzadeh, S.H. Rad, G. Naderi, M.R. Saeb, M. Mozafari, U.S. Schubert, Chitosan-based inks for 3D printing and bioprinting, Green Chem. 24 (1) (2022) 62–101, https://doi.org/10.1039/D1GC01799C.
[19] V.K. Mourya, N.N. Inamdar, Chitosan-modifications and applications: opportunities galore, React. Funct. Polym. 68 (6) (2008) 1013–1051, https://doi.org/10.1016/j.reactfunctpolym.2008.03.002.
[20] M. Vakili, M. Rafatullah, B. Salamatinia, A.Z. Abdullah, M.H. Ibrahim, K.B. Tan, Z. Gholami, P. Amouzgar, Application of chitosan and its derivatives as adsorbents for dye removal from water and wastewater: a review, Carbohydr. Polym. 113 (2014) 115–130, https://doi.org/10.1016/j.carbpol.2014.07.007.
[21] C. Brasselet, G. Pierre, P. Dubessay, M. Dols-Lafargue, J. Coulon, J. Maupeu, A. Vallet-Courbin, H. de Baynast, T. Doco, P. Michaud, C. Delattre, Modification of chitosan for the generation of functional derivatives, Appl. Sci. 9 (7) (2019) 1321, https://doi.org/10.3390/app9071321.
[22] P.S. Bakshi, D. Selvakumar, K. Kadirvelu, N.S. Kumar, Chitosan as an environment friendly biomaterial – a review on recent modifications and applications, Int. J. Biol. Macromol. 150 (2020) 1072–1083, https://doi.org/10.1016/j.ijbiomac.2019.10.113.
[23] N.A. Negm, H.H.H. Hefni, A.A.A. Abd-Elaal, E.A. Badr, M.T.H. Abou Kana, Advancement on modification of chitosan biopolymer and its potential applications, Int. J. Biol. Macromol. 152 (2020) 681–702, https://doi.org/10.1016/j.ijbiomac.2020.02.196.
[24] B. Qu, Y. Luo, Chitosan-based hydrogel beads: preparations, modifications and applications in food and agriculture sectors – a review, Int. J. Biol. Macromol. 152 (2020) 437–448, https://doi.org/10.1016/j.ijbiomac.2020.02.240.
[25] X. Ai, F. Pan, Z. Yang, J. Li, T. Tuersuntuoheti, O. Wang, L. Zhao, L. Zhao, Computational design of a chitosan derivative for improving the color stability of anthocyanins: theoretical calculation and experimental verification, Int. J. Biol. Macromol. 219 (2022) 721–729, https://doi.org/10.1016/j.ijbiomac.2022.08.051.
[26] A.M. Bayoumy, A. Refaat, I.S. Yahia, H.Y. Zahran, H. Elhaes, M.A. Ibrahim, M. Shkir, Functionalization of graphene quantum dots (GQDs) with chitosan biopolymer for biophysical applications, Opt. Quant. Electron. 52 (1) (2019) 16, https://doi.org/10.1007/s11082-019-2134-z.
[27] B.H. Morrow, G.F. Payne, J. Shen, pH-responsive self-assembly of polysaccharide through a rugged energy landscape, J. Am. Chem. Soc. 137 (40) (2015) 13024–13030, https://doi.org/10.1021/jacs.5b07761.
[28] M.T. McDonnell, D.A. Greeley, K.M. Kit, D.J. Keffer, Molecular dynamics simulations of hydration effects on solvation, diffusivity, and permeability in chitosan/chitin films, J. Phys. Chem. B 120 (34) (2016) 8997–9010, https://doi.org/10.1021/acs.jpcb.6b05999.
[29] C.-C. Tsai, B.H. Morrow, W. Chen, G.F. Payne, J. Shen, Toward understanding the environmental control of hydrogel film properties: how salt modulates the flexibility of chitosan chains, Macromolecules 50 (15) (2017) 5946–5952, https://doi.org/10.1021/acs.macromol.7b01116.

[30] C.H. Borca, C.A. Arango, Molecular dynamics of a water-absorbent nanoscale material based on chitosan, J. Phys. Chem. B 120 (15) (2016) 3754–3764, https://doi.org/10.1021/acs.jpcb.5b11230.
[31] J. Cui, Z. Yu, D. Lau, Effect of acetyl group on mechanical properties of chitin/chitosan nanocrystal: a molecular dynamics study, Int. J. Mol. Sci. 17 (1) (2016) 61, https://doi.org/10.3390/ijms17010061.
[32] E.F. Franca, L.C.G. Freitas, R.D. Lins, Chitosan molecular structure as a function of N-acetylation, Biopolymers 95 (7) (2011) 448–460, https://doi.org/10.1002/bip.21602.
[33] W. Zhao, W. Zou, F. Liu, F. Zhou, N.E. Altun, Molecular dynamics simulations of the solubility and conformation change of chitosan grafted polyacrylamide: impact of grafting rate, J. Mol. Graph. Model. 126 (2024) 108660, https://doi.org/10.1016/j.jmgm.2023.108660.
[34] N. D'Amelio, C. Esteban, A. Coslovi, L. Feruglio, F. Uggeri, M. Villegas, J. Benegas, S. Paoletti, I. Donati, Insight into the molecular properties of chitlac, a chitosan derivative for tissue engineering, J. Phys. Chem. B 117 (43) (2013) 13578–13587, https://doi.org/10.1021/jp4067263.
[35] P.M.C. Matias, J.F.M. Sousa, E.F. Bernardino, J.P. Vareda, L. Durães, P.E. Abreu, J. M.C. Marques, D. Murtinho, A.J.M. Valente, Reduced chitosan as a strategy for removing copper ions from water, Molecules 28 (10) (2023) 4110, https://doi.org/10.3390/molecules28104110.
[36] M. Khajavian, S. Shahsavarifar, E. Salehi, V. Vatanpour, M. MasteriFarahani, F. Ghaffari, S.A. Tabatabaei, Ethylenediaminefunctionalized ZIF-8 for modification of chitosan-based membrane adsorbents: batch adsorption and molecular dynamic simulation, Chem. Eng. Res. Des. 175 (2021) 131–145, https://doi.org/10.1016/j.cherd.2021.08.033.
[37] D.S. Chauhan, K.R. Ansari, A.A. Sorour, M.A. Quraishi, H. Lgaz, R. Salghi, Thiosemicarbazide and thiocarbohydrazide functionalized chitosan as ecofriendly corrosion inhibitors for carbon steel in hydrochloric acid solution, Int. J. Biol. Macromol. 107 (2018) 1747–1757, https://doi.org/10.1016/j.ijbiomac.2017.10.050.
[38] M. Khnifira, W. Boumya, M. Abdennouri, M. Sadiq, M. Achak, G. Serdaroğlu, S. Kaya, S. Şimşek, N. Barka, A combined molecular dynamic simulation, DFT calculations, and experimental study of the eriochrome black T dye adsorption onto chitosan in aqueous solutions, Int. J. Biol. Macromol. 166 (2021) 707–721, https://doi.org/10.1016/j.ijbiomac.2020.10.228.
[39] A. Khezri, A. Karimi, F. Yazdian, M. Jokar, S.R. Mofradnia, H. Rashedi, Z. Tavakoli, Molecular dynamic of curcumin/chitosan interaction using a computational molecular approach: emphasis on biofilm reduction, Int. J. Biol. Macromol. 114 (2018) 972–978, https://doi.org/10.1016/j.ijbiomac.2018.03.100.
[40] S.W. Benner, V.T. John, C.K. Hall, Simulation study of hydrophobically modified chitosan as an oil dispersant additive, J. Phys. Chem. B 119 (23) (2015) 6979–6990, https://doi.org/10.1021/acs.jpcb.5b01092.
[41] A. Singhal, J.D. Schneible, R.L. Lilova, C.K. Hall, S. Menegatti, A. Grafmüller, A multiscale coarse-grained model to predict the molecular architecture and drug transport properties of modified chitosan hydrogels, Soft Matter 16 (47) (2020) 10591–10610, https://doi.org/10.1039/D0SM01243B.
[42] A. Avdoshin, V. Naumov, L.C. Ciacchi, S. Ignatov, S. Köppen, Atomistic simulations of chitosan as a possible carrier system for miRNA transport, Mater. Adv. 4 (4) (2023) 1113–1124, https://doi.org/10.1039/D2MA00830K.
[43] M. Przybyłek, P. Bełdowski, F. Wieland, P. Cysewski, A. Sionkowska, Collagen type II—chitosan interactions as dependent on hydroxylation and acetylation inferred from molecular dynamics simulations, Molecules 28 (1) (2023) 154, https://doi.org/10.3390/molecules28010154.
[44] J. Razzokov, P. Marimuthu, K. Saidov, O. Ruzimuradov, S. Mamatkulov, Penetration of chitosan into the single walled armchair carbon nanotubes: atomic scale insight, Crystals 11 (10) (2021) 1174, https://doi.org/10.3390/cryst11101174.
[45] W. Martin, W. Zhu, G. Krilov, Simulation study of noncovalent hybridization of carbon nanotubes by single-stranded DNA in water, J. Phys. Chem. B 112 (50) (2008) 16076–16089, https://doi.org/10.1021/jp8040567.
[46] T. Zhang, Z. Wu, H. Zhu, Z. Wang, S. Sun, S., Hu, pH/temperatureresponsive salt-tolerant Pickering emulsion formed by PNIPAMmodified chitosan particles, Colloids Surf. A Physicochem. Eng. Asp. 657 (2023) 130548, https://doi.org/10.1016/j.colsurfa.2022.130548.
[47] M. Ziegler-Borowska, D. Chełminiak, H. Kaczmarek, A. KaczmarekKędziera, Effect of side substituents on thermal stability of the modified chitosan and its nanocomposites with magnetite, J. Therm. Anal. Calorim. 124 (3) (2016) 1267–1280, https://doi.org/10.1007/s10973-016-5260-x.
[48] O. Guvench, S.S. Mallajosyula, E.P. Raman, E. Hatcher, K. Vanommeslaeghe, T. J. Foster, F.W. Jamison, A.D. MacKerell, CHARMM additive all-atom force field for carbohydrate derivatives and its utility in polysaccharide and carbohydrate–protein modeling, J. Chem. Theory Comput. 7 (10) (2011) 3162–3180, https://doi.org/10.1021/ct200328p.
[49] CHARMM Force Field Files. https://mackerell.umaryland.edu/charmm_ff.shtml, Nov. 2017.
[50] K. Vanommeslaeghe, E. Hatcher, C. Acharya, S. Kundu, S. Zhong, J. Shim, E. Darian, O. Guvench, P. Lopes, I. Vorobyov, A.D. MacKerell, CHARMM General Force Field (CGenFF): a force field for drug-like molecules compatible with the CHARMM all-atom additive biological force fields, J. Comput. Chem. 31 (4) (2010) 671–690, https://doi.org/10.1002/jcc.21367.
[51] K. Vanommeslaeghe, A.D. MacKerell, Automation of the CHARMM General Force Field (CGenFF) I: bond perception and atom typing, J. Chem. Inf. Model. 52 (12) (2012) 3144–3154, https://doi.org/10.1021/ci300363c.
[52] K. Vanommeslaeghe, E.P. Raman, A.D. MacKerell, Automation of the CHARMM General Force Field (CGenFF) II: assignment of bonded parameters and partial atomic charges, J. Chem. Inf. Model. 52 (12) (2012) 3155–3168, https://doi.org/10.1021/ci3003649.
[53] J.C. Phillips, R. Braun, W. Wang, J. Gumbart, E. Tajkhorshid, E. Villa, C. Chipot, R. D. Skeel, L. Kalé, K. Schulten, Scalable molecular dynamics with NAMD, J. Comput. Chem. 26 (16) (2005) 1781–1802, https://doi.org/10.1002/jcc.20289.
[54] W. Humphrey, A. Dalke, K. Schulten, VMD: visual molecular dynamics, J. Mol. Graph. 14 (1) (1996) 33–38, https://doi.org/10.1016/02637855(96)00018-5.
[55] R. Naohara, S. Namai, J. Kamiyama, T. Ikeda-Fukazawa, Structure and diffusive properties of water in polymer hydrogels, J. Phys. Chem. B 126 (40) (2022) 7992–7998, https://doi.org/10.1021/acs.jpcb.2c03069.
[56] A.-T. Kuo, T. Sonoda, S. Urata, R. Koguchi, S. Kobayashi, M. Tanaka, Elucidating the feature of intermediate water in hydrated poly($_m$methoxyalkyl acrylate)s by molecular dynamics simulation and differential scanning calorimetry measurement, ACS Biomater. Sci. Eng. 6 (7) (2020) 3915–3924, https://doi.org/10.1021/acsbiomaterials.0c00746.